(b) The K^+N total cross sections exhibit at least two structures, one in each isotopic spin state. A conclusive interpretation is at present not possible.

(c) The analysis of the π-meson data throws some light on and points out the limitations of the analysis of experimental data using neutron targets bound in the deuteron.

(d) The availability of a reasonably intense and pure K-meson beam makes the precise measurement of total cross sections a powerful tool for investigating the existence and determining some of the properties of strange-baryon resonances.

(e) Of the above-mentioned new structures, the Y_0^* (2107), Y_1^* (1912), Y_1^* (2025), Z_1^* (1900), and Z_0^* (1780) have already been confirmed by independent measurements.[19,21,42,43]

ACKNOWLEDGMENTS

We wish to thank Dr. G. K. Green, Dr. J. R. Sanford, T. Blair, and the AGS staff for their support. We thank Dr. A. Ashmore, Dr. A. Mueller, Dr. R. Peierls, and Dr. L. Stodolsky for useful discussions and Dr. R. J. Abrams and Dr. D. N. Michael for their assistance in data analysis. The cooperation of A. P. Schlafke and the Cryogenic Group is greatly appreciated. We also wish to acknowledge the aid of J. Fuhrmann and the technical assistance of P. Anzoli, G. Munoz, H. Sauter, F. Seier, and O. Thomas.

PHYSICAL REVIEW D VOLUME 1, NUMBER 7 1 APRIL 1970

Total Cross Sections of $K^{\pm}$ Mesons and Antiprotons on Nucleons up to 3.3 GeV/c†

R. J. Abrams, R. L. Cool, G. Giacomelli,* T. F. Kycia, B. A. Leontic,‡ K. K. Li, and D. N. Michael
Brookhaven National Laboratory, Upton, New York 11973

(Received 8 October 1969)

Total cross sections of $K^{\pm}$ and $\bar{p}$ on hydrogen and deuterium were measured in a standard transmission experiment with statistical precisions of the order of 0.05–0.25%. Data were obtained in the momentum range 2.45–3.30 GeV/c for K^-N, 1.55–3.30 GeV/c for K^+N, and 1.00–3.30 GeV/c for $\bar{p}N$. Cross sections for the pure isotopic spin states are obtained using a procedure for the deuterium data which takes into account Fermi motion and the shadow effect. Evidence for the following new structures was found: $Y_1^*(2455)$, $Y_1^*(2620)$, $Y_0^*(2585)$, $Z_1^*(2150)$, $Z_1^*(2500)$, $\pi_1^*(2190)$, $\pi_1^*(2350)$, and $\pi_0^*(2375)$.

I. INTRODUCTION

MEASUREMENTS of kaon-nucleon total cross sections have been performed with high enough precision to detect several new strange-baryon resonances.[1–4] The availability of partially separated beams of sufficient purity and intensity has made it possible to extend these measurements to higher energy as well as to perform new measurements of antiproton-nucleon total cross sections. In the present paper we describe a search for higher-mass baryon resonances with strangeness ± 1 and for high-mass nonstrange boson resonances using the total cross-section method.

In this experiment, the total cross sections were measured in hydrogen and deuterium with K^- mesons from 2.45 to 3.30 GeV/c laboratory momentum, with K^+ mesons from 1.55 to 3.30 GeV/c, and with antiprotons from 1.00 to 3.30 GeV/c. The measurements were performed at 50-MeV/c intervals with a point-to-point statistical accuracy ranging from 0.05 to 0.25%. Preliminary results of the experiment have already been published.[2–4]

In searching for new resonances, the total cross section is the least sensitive formation experiment, but it can be carried out to a very high statistical accuracy which compensates for its poor intrinsic sensitivity. If a structure is found, the measurement can yield information on the mass, isotopic spin, width, and height from which one obtains the product of spin and elasticity.[1] The interpretation of a structure in the total cross section, however, is not unique: it could be the result of a resonance or a threshold effect.

We shall give the description of the experiment in Sec. II, corrections and uncertainties in the data in Sec. III, and the experimental results in Sec. IV. Throughout the present paper, we shall refer to I[1] for

† Work performed under the auspices of the U. S. Atomic Energy Commission.

* On leave of absence from the University of Bologna, Bologna, Italy.

‡ Present address: Institut za Fiziku Sveucilista, Zagreb, Yugoslavia.

[1] R. L. Cool, G. Giacomelli, T. F. Kycia, B. A. Leontic, K. K. Li, A. Lundby, J. Teiger, and C. Wilkin, preceding paper, Phys. Rev. D 1, 1887 (1970). This paper is referred to throughout the text as I.

[2] R. J. Abrams, R. L. Cool, G. Giacomelli, T. F. Kycia, B. A. Leontic, K. K. Li, and D. N. Michael, Phys. Rev. Letters 18, 1209 (1967).

[3] R. J. Abrams, R. L. Cool, G. Giacomelli, T. F. Kycia, B. A. Leontic, K. K. Li, and D. N. Michael, Phys. Rev. Letters 19, 259 (1967).

[4] R. J. Abrams, R. L. Cool, G. Giacomelli, T. F. Kycia, B. A. Leontic, K. K. Li, and D. N. Michael, Phys. Rev. Letters 19, 678 (1967).

a more complete discussion of the principle of measurement, for more details about the experiment and data analysis, and for a more complete list of references.

Several new structures have been found in this experiment; their properties are listed in Table VIII (below).

II. DESCRIPTION OF EXPERIMENT

A. Beam

The experiment was carried out in a partially separated beam (Fig. 1) at Brookhaven National Laboratory's Alternating Gradient Synchrotron (AGS). The beam was similar to that described in I, except that the longer, higher-momentum branch was used. The K mesons and antiprotons were produced in an internal target in the G10 straight section. The target was a 1-mm-diam×13-mm-long beryllium wire aligned along the beam direction, which was at 10° to the circulating proton beam. The small size of the wire resulted in essentially a point source of secondary particles. The quadrupole triplet Q_1, Q_2, and Q_3 formed a beam parallel vertically and slightly converging horizontally. Particles of the desired momentum were deflected 6° by D_1 into two 15-ft-long electrostatic separators with a vertical aperture of 4 in. and a horizontal aperture of 10 in. The voltage on the gap was maintained at between 400 and 430 kV. The angular acceptance of the beam was defined to be $\Delta\theta_V = \pm 9$ mrad and $\Delta\theta_H = \pm 14$ mrad by a collimator between D_1 and the rectangular beam separator. In the present experiment, the switching magnet D_2 was turned off, and the quadrupole doublet Q_4 and Q_5 focused the beam horizontally at the sextupole and vertically at the mass slit. The momentum spread in the beam was set at $\pm 0.75\%$ by means of Hevimet slits near the sextupole. The mass slit was constructed of Hevimet and had a vertical aperture of 0.14 in. and a horozontal aperture of 8 in. The vertical beam size at the mass slit was about 0.13 in. full width at half-height. The bending magnet D_3, which deflected the beam by 6°, recombined momenta and removed the low momentum components produced at the mass slit. The quadrupole triplet Q_6, Q_7, and Q_8 formed a final image at the transmission counters which was about 2 in. vertically and 2.5 in. horizontally. The total length of the beam to the final focus was 49 m.

The separation between K and π images at the mass slit was 0.22 in. at 1.9 GeV/c, but decreased to 0.08 in. at 3.3 GeV/c: thus, between 2.4 and 3.3 GeV/c, the π-to-K ratio varied between 15:1 and 30:1. In order to maintain the background below one part in a thousand in the K-meson identification, a focusing gas differential Čerenkov counter was used. With a typical circulating beam of 10^{12} protons on the internal target, the K^+-meson flux above 2.4 GeV/c was about 15 000 per pulse. At the lowest momentum used in the long branch, 1.55 GeV/c, the flux was about 3500 per pulse. The K^--meson fluxes were typically about one-third of the K^+-meson fluxes.

The separation for antiprotons was large over the range of the experiment; the π-meson–to–antiproton ratio in the beam was below 2:1 for momenta less than 2.8 GeV/c, above which it increased gradually to a value of 8:1 at 3.3 GeV/c. The contamination from other particles was kept below one part per thousand at all momenta by identifying the antiprotons with a liquid differential Čerenkov counter and time of flight. The flux varied from a maximum of 20 000 per pulse at 2.9 GeV/c to a minimum of 1000 per pulse at 1.0 GeV/c, with a typical circulating beam of 10^{12} protons on target.

B. Experimental Arrangement

Figure 2 shows the experimental arrangement. The beam was incident from the left. The beam telescope consists of counters S_1, S_2, and S_3, an anticoincidence counter $\bar{G}$, for rejecting particles outside the beam, and the focusing gas differential Čerenkov counter[5] which selected the wanted particles in the beam. The gas counter was replaced by a liquid differential Čerenkov counter[6] when antiproton cross sections were measured and when K^+-meson cross sections were measured for momenta below 2.3 GeV/c; this was the same counter that was used in I. Both counters provided a coincidence output for the wanted particles, as well as an anticoincidence output for faster particles. In the liquid counter, four different radiators, varying in index of refraction between 1.25 and 1.50, were used to cover the antiproton velocity range $\beta = 0.96$–0.74. Antiprotons were further identified by time of flight over the path S_1S_2 (10.5 m). The time-of-flight requirement was achieved by offsetting the S_1S_2 relative delay to about 0.5 nsec from the edge of the antiproton delay curve.

The hydrogen, deuterium, and dummy targets were mounted side by side on a frame which rolled on rails, so that each target could easily be positioned on the beam line. The hydrogen and deuterium targets were 93.3 cm long and were in thermal contact with an outer jacket of liquid hydrogen, which provided a stable density in the targets of $\pm 0.05\%$. Absolute uncertainty in the density is probably $\pm 0.05\%$ for hydrogen and should be less than $\pm 0.25\%$ for deuterium. The dummy target simulated the material surrounding the hydrogen and deuterium. The density values used to compute the total cross sections were 0.0700 ± 0.0001 g/cm^3 for hydrogen and 0.1691 ± 0.0005 g/cm^3 for deuterium.

The cross section of the particles was determined from their transmission measured alternatively in the hydrogen, deuterium, and dummy targets. The transmission counters S_4 to S_{10} (shown in Fig. 2) subtended at the target solid angles of between 1.85 and 20.17 msr. The counter S_{11} was used to check the efficiency of the

[5] T. F. Kycia (unpublished).
[6] B. A. Leontic and J. Tieger, Brookhaven National Laboratory Internal Report No. BNL-50031 (T-447) (unpublished).

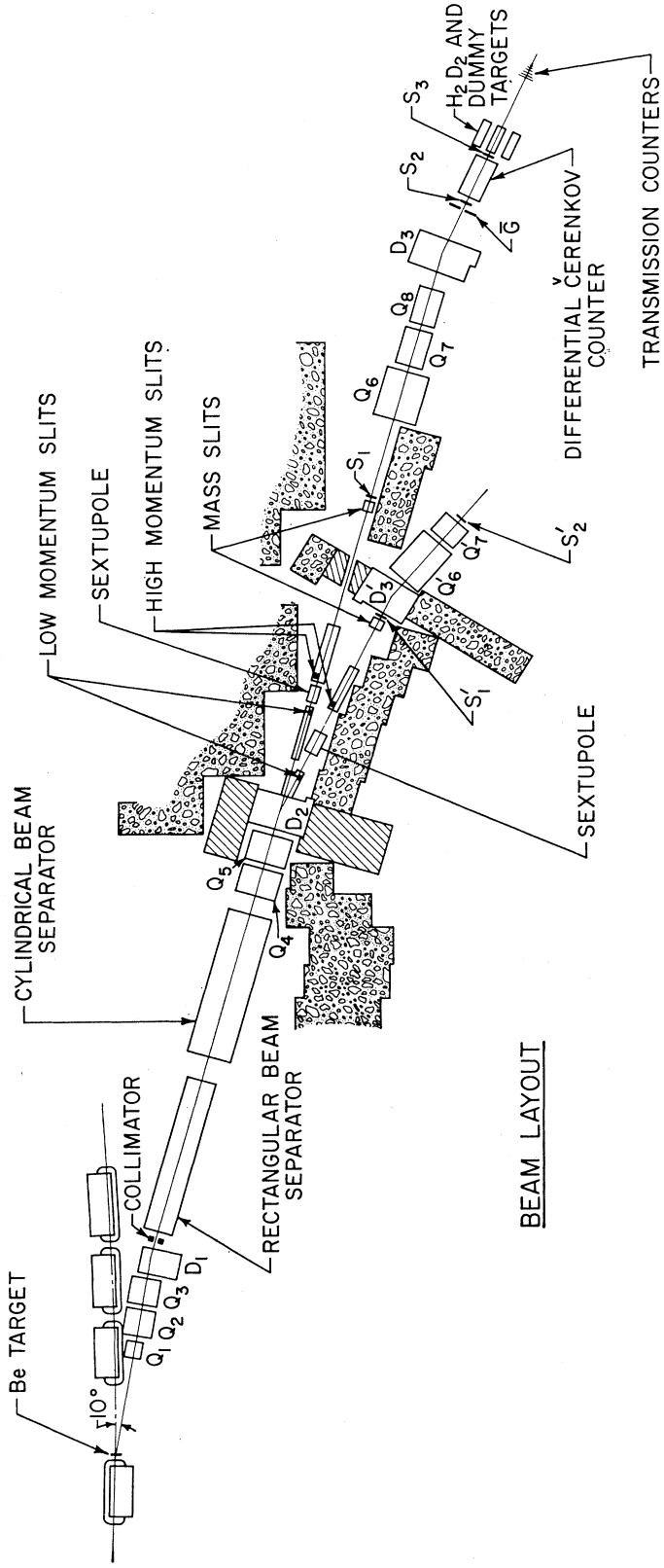

FIG. 1. Layout of the partially separated beam. Q_1–Q_8 are quadrupoles; D_1–D_3 are bending magnets; S_1–S_3 and $\tilde{G}$ are scintillation counters.

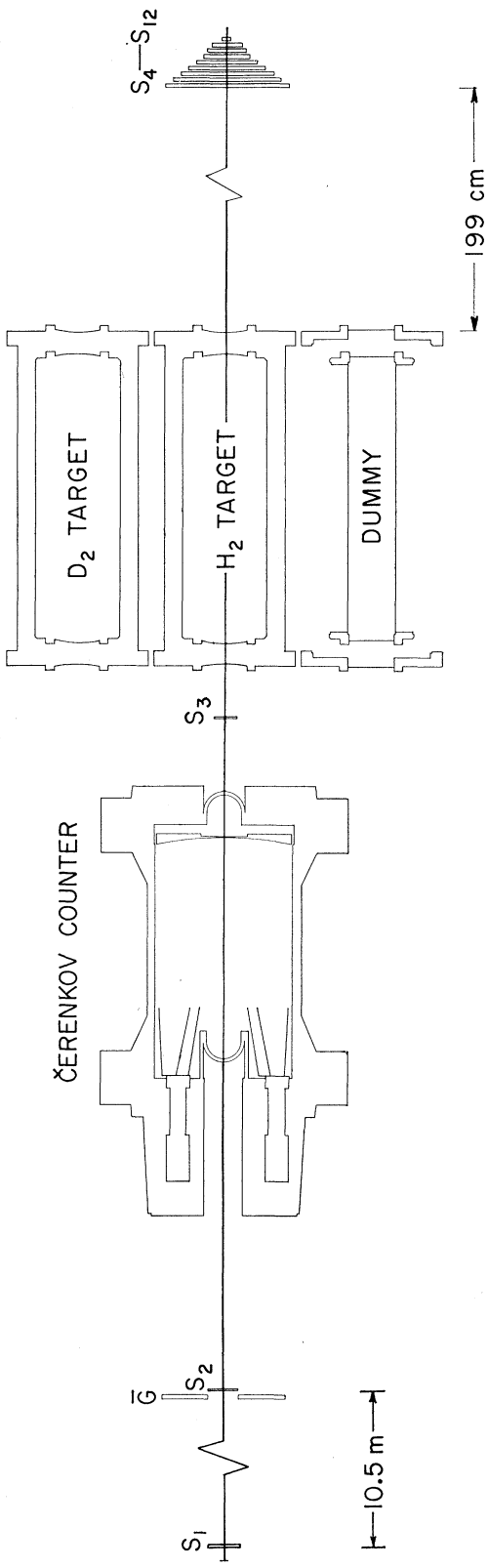

FIG. 2. Layout of the experimental apparatus. S_1, S_2, S_3, and $\bar{G}$ are scintillation counters defining the beam. The gas differential Čerenkov counter is shown; it was replaced by a liquid differential Čerenkov counter for some measurements at lower momenta. H_2, D_2, and the dummy are the liquid hydrogen, liquid deuterium, and dummy targets, respectively. S_4–S_{12} are the transmission counters.

transmission counters, and S_{12} was used for tuning the beam. The sizes of these counters were the same as in I.

Standard Brookhaven National Laboratory electronics (HEEP circuitry) was used; the electronic logic was the same as that used in I. Coincidence-anticoincidence circuitry counted the total beam flux $S=S_1S_2S_3\bar{G}$ and the flux of wanted particles $SC\bar{C}$, where C and $\bar{C}$ were the coincidence and anticoincidence outputs of the Čerenkov counter. The coincidence signal S was set to ignore a beam particle if it was preceded by another beam particle within 100 nsec in order to eliminate scalar-dead-time effects. The signal $SC\bar{C}$ was taken in coincidence with each of the transmission counters and each of the individual coincidences was scaled. The data were read at the end of each run directly onto punched paper tape, transferred to punch cards, and processed by a CDC 6600 computer.

C. Experimental Procedure

In the present experiment, the same experimental procedure that was used in I was followed. Data were obtained at 50-MeV/c intervals (except for a small region in which antiproton data were taken at 25-MeV/c intervals). Data were taken in the order of decreasing momentum; some points were measured twice as a check on reproducibility. After tuning the beam for the desired momentum and tuning the Čerenkov counter for the desired incident particle, data were typically taken in the sequence

$$EHHEDDEHHEDDEHHEDDE,$$

where E, H, and D denote runs with dummy, hydrogen, and deuterium targets, respectively. The efficiency of each transmission counter was checked before and after running at each momentum. For each particle, absorption cross sections on copper and carbon were also measured. The fact that these cross sections exhibited a smooth momentum dependence in each case added to the confidence that small structures in the hydrogen and deuterium cross sections were not being caused by instrumental effects. In order to keep accidental effects negligible, the total beam intensity in the S telescope was never allowed to be more than 150 000 particles per machine burst, with a smooth beam spill of at least 400 msec.

III. DETERMINATION OF TOTAL CROSS SECTIONS

A. Extrapolation Procedure

The ith transmission counter measures a cross section σ_i, which is

$$\sigma_i=(A/\rho_t LN)\ln(R_0/R), \tag{1}$$

where A is the atomic weight of the target material, ρ_t is its density, L is the target length, N is Avogadro's number, and R_0 and R are the fractions of beam reaching the ith transmission counter through the empty and full targets, respectively. σ_i is the total cross section σ_T minus the cross section for having a charged secondary in the solid angle subtended by the ith counter;

$$\sigma_i=\sigma_T-\int_{t_i}^{0}\frac{d\sigma(t)}{dt}dt, \tag{2}$$

where t is the four-momentum transfer to the target particle and $d\sigma/dt$ is the effective differential cross section. It equals the differential elastic cross section plus a contribution from the fraction of the inelastic cross section which gives a charged secondary forward. For the small t range covered by the transmission counters, the elastic cross section is known to fall off exponentially with t:

$$(d\sigma/dt)_{\rm el}=ae^{bt}\simeq a(1+bt). \tag{3}$$

The inelastic cross section changes more slowly with t. Assuming that

$$(d\sigma/dt)_{\rm in}\simeq c(1+et), \tag{4}$$

we obtain for Eq. (1)

$$\begin{aligned}\sigma_i&=\sigma_T+(a+c)t+\tfrac{1}{2}a(b+ce/a)t^2\\&=\sigma_T+(a+c)t+\tfrac{1}{2}ab't^2.\end{aligned} \tag{5}$$

Equation (5) gives the relation between the coefficients of the extrapolation line and the parameters for forward elastic and inelastic differential cross sections. Formula (5) applies to nuclear scattering only; Coulomb scattering and Coulomb-nuclear interference effects must be removed before attempting to fit the data to Eq. (5). Above 2.5 GeV/c, the range of t values covered by our transmission counters is such that the approximations [(3) or (4)] are not adequate to represent the sharp diffraction scattering from the deuterium nuclei. In these cases, the diffraction scattering from deuterium was subtracted before the extrapolation was performed.[7]

A least-squares fit was made to the partial cross sections σ_i for each momentum using functions of the form

$$\sigma=A+Bt+Ct^2. \tag{6}$$

From Eq. (5), the total cross section $\sigma_T=A$. The transmission counters S_4–S_9 were used in the fitting. As a check, fits were made by eliminating the smallest counter (S_9); the values of the coefficients A, B, and C did not change outside the errors. This gives confidence in the extrapolation procedure; it also indicates that the smallest counter used was not seriously affected by multiple Coulomb scattering and beam size effects. The t range covered by the transmission counters is sufficiently large [-0.005 to -0.05 (GeV/c)^2] that the quadratic extrapolation is needed. A linear extrapolation

[7] R. J. Abrams, R. L. Cool, G. Giacomelli, T. F. Kycia, B. A. Leontic, K. K. Li, and D. N. Michael, Phys. Rev. D 1, 2477 (1970); K. F. Riley, *ibid.* D 1, 2481 (1970).

TABLE I. Typical values of corrections to the total cross sections. Within the quoted accuracy, the dummy target corrections, the decay corrections, and the single Coulomb scattering corrections are the same for both hydrogen and deuterium.

Laboratory momentum (GeV/c)	Corrections to data (mb) Dummy target	Decay	Single Coulomb	Coulomb-nuclear interference For hydrogen	For deuterium	Diffraction scattering from deuterium	Deuteron screening term (mb)
			K^- mesons				
2.5	+0.17	−0.38	−0.02	+0.05	+0.05	+0.03	1.84
3.0	+0.16	−0.26	−0.01	+0.04	+0.04	+0.11	1.70
3.3	+0.16	−0.22	−0.01	+0.03	+0.03	+0.15	1.62
			K^+ mesons				
1.55	+0.15	−1.02	−0.06	−0.30	−0.38	···	0.81
2.0	+0.14	−0.60	−0.03	−0.24	−0.30	···	0.79
2.5	+0.13	−0.38	−0.02	−0.18	−0.22	···	0.76
3.0	+0.13	−0.26	−0.01	−0.14	−0.18	···	0.74
3.3	+0.13	−0.22	−0.01	−0.12	−0.16	···	0.73
			Antiprotons				
1.0	+0.59	···	−0.15	−1.58	−2.94	···	24.31
1.5	+0.55	···	−0.06	−0.69	−1.23	···	20.31
2.0	+0.52	···	−0.03	−0.31	−0.52	+0.02	16.71
2.5	+0.49	···	−0.02	−0.14	−0.22	+0.21	13.78
3.0	+0.47	···	−0.01	−0.06	−0.08	+0.47	11.87
3.3	+0.46	···	−0.01	−0.03	−0.05	+0.70	11.01

would introduce a slowly varying systematic error of about 1–2%.

The coefficient $B=(a+c)$ turns out to be considerably larger than the value computed from the total cross sections via the optical theorem and dispersion relations, which indicates that there is a significant contribution from inelastic scattering. The coefficient b' defined in formula (5) is computed from C and a; it is appreciably different from the b coefficient determined from elastic scattering data, again indicating the importance of inelastic effects.

TABLE II. K^-p and K^-d total cross sections. Errors represent point-to-point statistical standard deviations only. The over-all systematic error is estimated to be less than ±1%.

Laboratory momentum (GeV/c)	$\sigma_T(K^-p)$ (mb)	$\sigma_T(K^-d)$ (mb)
2.35	29.44±0.05	52.43±0.10
2.40	29.10±0.05	52.19±0.07
2.45	28.87±0.07	51.99±0.07
2.50	28.46±0.06	51.75±0.06
2.55	28.30±0.06	51.62±0.06
2.60	28.21±0.06	51.37±0.06
2.65	28.10±0.06	51.12±0.06
2.70	28.02±0.06	50.84±0.06
2.75	27.83±0.06	50.59±0.06
2.80	27.72±0.07	50.33±0.07
2.85	27.73±0.06	50.28±0.06
2.90	27.58±0.06	50.05±0.06
2.95	27.51±0.06	49.90±0.06
3.00	27.42±0.06	49.81±0.06
3.05	27.20±0.06	49.54±0.06
3.10	27.00±0.06	49.27±0.07
3.15	26.98±0.06	49.23±0.06
3.20	26.78±0.07	48.74±0.10
3.25	26.70±0.07	48.59±0.07
3.30	26.73±0.06	48.68±0.06

B. Corrections and Uncertainties

Since the aim of the experiment was to search for new structure in the total cross sections, great care was exercised to avoid energy-dependent errors greater than about ±0.1%, whereas no great effort was made to obtain an absolute cross-section uncertainty to better than about ±1%.[7] The same corrections have been applied to the data that were described in I: dummy target correction, deuteron target contamination correction, decay correction, and single Coulomb and Coulomb-nuclear interference corrections. In addition, a correction was made for the diffraction scattering from deuterium mentioned in the previous section. Typical values for these corrections are given in Table I.

The dummy target correction resulted from the fact that the dummy had less material (primarily superinsulation) around it than the hydrogen or deuterium targets; hence, it caused less secondary scattering into the transmission counters. The correction was measured by comparing the transmission of the dummy with that of the empty hydrogen target at 2.50 GeV/c and was scaled up or down to other momenta according to the behavior of the carbon cross sections.

The deuteron target contamination correction was +0.15% to account for a measured contamination of 0.6 mole % of HD molecules in the liquid deuterium. No contamination corrections were necessary for the liquid hydrogen.

The decay correction for kaons arose from the difference in momentum loss between dummy and full targets and, as a consequence, the difference in decay probabilities for the two cases.

It was also necessary to correct for single Coulomb scattering and for Coulomb-nuclear interference.

The uncertainty in the Coulomb-nuclear interference corrections for the antiproton-deuterium data is especially large because nothing is known about the values of ρ_n, the ratio of the real part to the imaginary part of the forward antiproton-neutron scattering amplitude. For the present calculations, we have (arbitrarily) assumed $\rho_n=\rho_p$, where ρ_p, the ratio for forward antiproton-proton scattering, was computed from dispersion relations.[8]

For kaons, the extrapolated values at $t=0$ were typically 0.5–2 mb higher than the partial cross sections measured by the smallest counter used in the extrapolations; for antiprotons they were typically 2–5 mb higher. The statistical error introduced by the extrapolation procedure is negligible, while the systematic error is very likely the single largest uncertainty contributing to the scale error.

The absolute uncertainty in beam momentum may be as high as $\pm 0.5\%$, while the relative precision between neighboring points is about 0.1–0.2%. The experimental energy resolution arises from the finite target length (93.3 cm) and finite beam momentum resolution ($\pm 0.75\%$), and was about 15 MeV in the center-of-mass system, full width at half-maximum, for both kaons and antiprotons over the energy range of the present experiment.

TABLE III. K^+p and K^+d total cross sections. Errors represent point-to-point statistical standard deviations only. The over-all systematic error is estimated to be less than $\pm 1\%$.

Laboratory momentum (GeV/c)	$\sigma_T(K^+p)$ (mb)	$\sigma_T(K^+d)$ (mb)
1.55	17.70±0.11	36.03±0.11
1.60	17.71±0.10	35.94±0.11
1.70	17.73±0.08	35.78±0.08
1.75	17.83±0.07	35.90±0.09
1.80	17.98±0.10	35.68±0.10
1.85	17.77±0.07	35.63±0.07
1.90	17.79±0.07	35.70±0.07
1.95	17.75±0.07	35.69±0.06
2.00	17.63±0.06	35.68±0.05
2.05	17.72±0.07	35.55±0.07
2.10	17.56±0.07	35.34±0.08
2.15	17.57±0.07	35.28±0.07
2.20	17.60±0.07	35.28±0.07
2.30	17.44±0.06	34.98±0.07
2.35	17.52±0.04	35.05±0.06
2.40	17.56±0.06	34.92±0.06
2.45	17.48±0.04	35.00±0.05
2.50	17.49±0.05	34.87±0.06
2.55	17.44±0.04	34.87±0.04
2.60	17.50±0.04	34.85±0.05
2.65	17.47±0.04	34.75±0.05
2.70	17.41±0.04	34.77±0.04
2.75	17.41±0.04	34.72±0.05
2.80	17.40±0.04	34.67±0.05
2.85	17.30±0.04	34.52±0.05
2.90	17.34±0.03	34.48±0.04
2.95	17.30±0.04	34.42±0.04
3.00	17.19±0.04	34.35±0.04
3.05	17.14±0.04	34.34±0.04
3.10	17.08±0.05	34.30±0.04
3.15	17.15±0.04	34.14±0.04
3.20	17.13±0.03	34.12±0.04
3.25	17.13±0.03	34.20±0.04
3.30	17.14±0.03	34.13±0.04

TABLE IV. $\bar{p}p$ and $\bar{p}d$ total cross sections. Errors represent point-to-point statistical standard deviations only. The over-all systematic error is estimated to be less than $\pm 1\%$.

Laboratory momentum (GeV/c)	$\sigma_T(\bar{p}p)$ (mb)	$\sigma_T(\bar{p}d)$ (mb)
1.00	117.42±0.21	208.18±0.21
1.05	114.59±0.17	203.37±0.20
1.10	111.64±0.16	199.84±0.19
1.15	110.11±0.12	197.14±0.15
1.20	108.96±0.11	195.21±0.13
1.25	107.75±0.10	193.77±0.13
1.30	106.47±0.10	191.71±0.12
1.345	105.50±0.10	190.17±0.12
1.40	102.78±0.09	186.19±0.12
1.45	101.12±0.08	183.51±0.10
1.49	100.26±0.06	181.47±0.09
1.55	98.82±0.06	178.80±0.08
1.60	97.81±0.06	176.97±0.08
1.65	97.05±0.06	175.16±0.08
1.70	96.46±0.06	173.75±0.08
1.75	95.61±0.06	172.33±0.08
1.806	94.48±0.06	169.88±0.07
1.85	93.71±0.06	168.49±0.09
1.875	93.05±0.06	167.55±0.07
1.90	92.52±0.06	166.59±0.07
1.925	92.07±0.06	165.69±0.07
1.95	91.38±0.06	164.59±0.07
2.00	90.23±0.04	162.69±0.06
2.05	88.84±0.05	160.46±0.07
2.095	88.46±0.06	159.99±0.07
2.15	87.39±0.06	157.76±0.07
2.20	86.81±0.06	156.45±0.07
2.25	85.62±0.06	154.53±0.07
2.30	85.00±0.05	153.13±0.07
2.35	84.45±0.05	152.24±0.07
2.40	83.66±0.06	150.56±0.07
2.45	83.16±0.06	149.46±0.07
2.50	82.32±0.04	148.21±0.05
2.55	81.64±0.05	147.09±0.07
2.60	81.12±0.05	145.93±0.07
2.65	80.61±0.05	145.01±0.06
2.70	79.90±0.05	143.99±0.06
2.75	79.47±0.05	143.12±0.07
2.80	78.91±0.05	141.90±0.06
2.85	78.21±0.05	140.87±0.06
2.90	77.79±0.05	140.03±0.06
2.95	77.23±0.05	139.19±0.06
3.00	76.68±0.05	138.25±0.06
3.05	76.29±0.05	137.30±0.06
3.10	75.66±0.05	136.37±0.06
3.15	75.16±0.05	135.70±0.06
3.20	74.66±0.05	134.84±0.06
3.25	74.20±0.05	134.05±0.06
3.30	73.67±0.05	133.23±0.06

IV. RESULTS

A. Measured Cross Sections

The experimental results for K^--p, K^--d, K^+-p, K^+-d, $\bar{p}$-p, and $\bar{p}$-d total cross sections are listed in Tables II–IV, and are plotted in Figs. 3–10. The agree-

[8] P. Söding, Phys. Letters 8, 285 (1964).

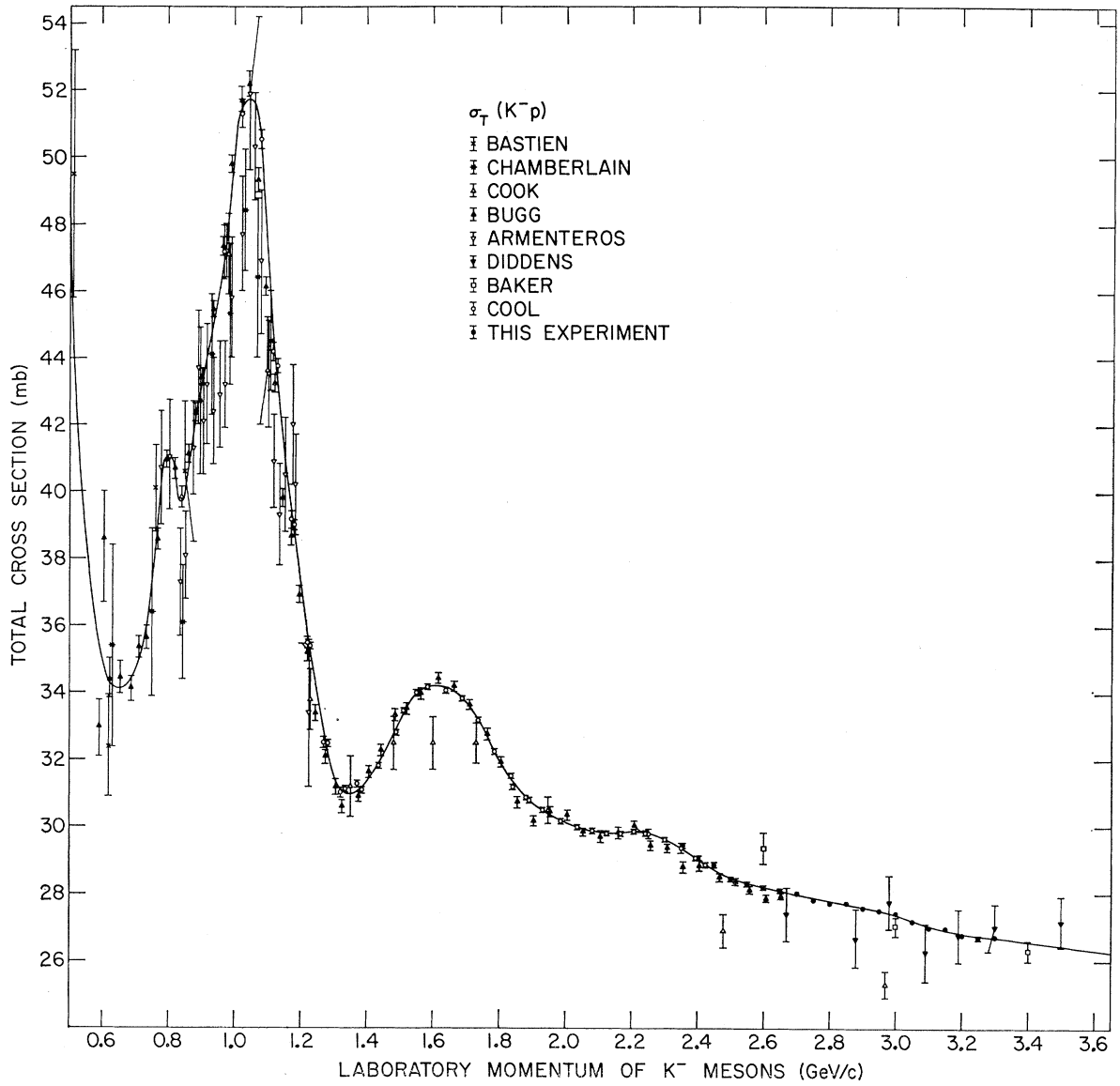

FIG. 3. K^--p total cross sections, 0.6–3.5 GeV/c.

ment with previous data is reasonable.[1,9–12] There are no pronounced enhancements in the data but only small structures or variations in slope.

In Figs. 3 and 4, the K^--p and K^--d total cross sections are displayed over the range 0.6–3.3 GeV/c. The data from the present experiment may be seen more clearly on the expanded scale of Figs. 5 and 6. The K^--p data exhibit two significant changes in slope, one at about 2.6 GeV/c and the other near 3.0 GeV/c. The K^--d data are suggestive of two small structures near the same two momentum values, but they are less pronounced, in part owing presumably to the smearing out effect of the Fermi momentum in the deuteron.

The K^+-p and K^+-d data (Figs. 7 and 8) exhibit two new small structures at laboratory momenta of about 1.8 and 2.7 GeV/c.

Two small bumps are clearly present in both $\bar{p}$-p and $\bar{p}$-d data (Figs. 9 and 10) at laboratory momenta of about 1.3 and 1.8 GeV/c.

B. Pure Isotopic-Spin Cross Sections

The measured cross sections can be expressed in terms of the total cross sections σ_0 and σ_1 in the pure

[9] B. Cork, G. R. Lambertson, O. Piccioni, and W. A. Wenzel, Phys. Rev. **107**, 248 (1957).
[10] R. Armenteros, C. A. Combes, B. Cork, G. R. Lambertson, and W. A. Wenzel, Phys. Rev. **119**, 2068 (1960).
[11] T. Elioff, L. Agnew, O. Chamberlain, H. M. Steiner, C. Weigand, and T. Ypsilantis, Phys. Rev. **128**, 869 (1962).
[12] V. Amaldi, Jr., T. Fazzini, G. Fidecaro, G. Ghesquiere, M. Legros, and H. Steiner, Nuovo Cimento **34**, 825 (1964).

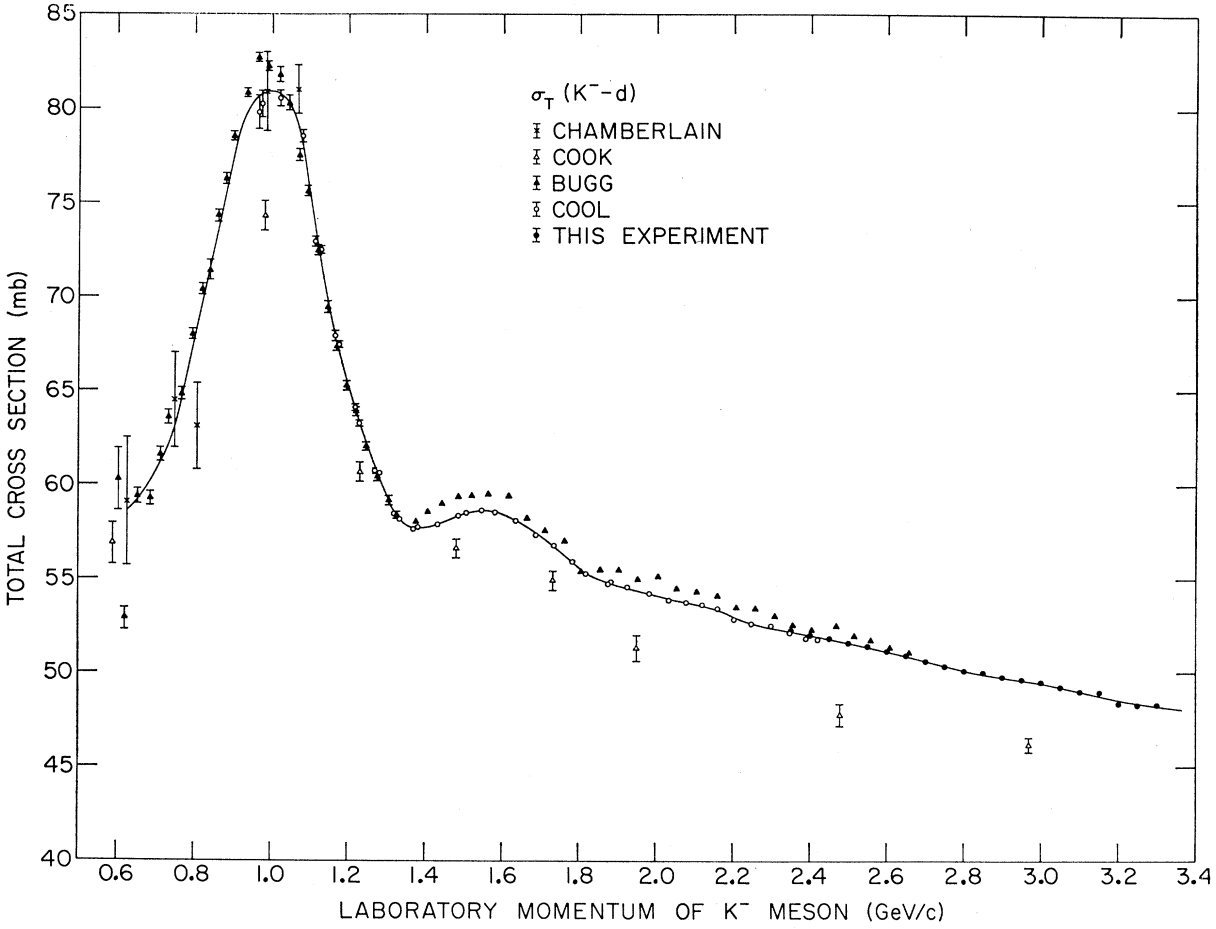

FIG. 4. K^--d total cross sections, 0.6–3.3 GeV/c.

isotopic spin states $I=0$ and $I=1$ for K^- mesons as

$$\sigma_{K^-p}=\tfrac{1}{2}(\sigma_0+\sigma_1), \tag{7}$$

$$\sigma_{K^-n}=\sigma_1, \tag{8}$$

and for K^+ mesons as

$$\sigma_{K^+p}=\sigma_1, \tag{9}$$

$$\sigma_{K^+n}=\tfrac{1}{2}(\sigma_0+\sigma_1). \tag{10}$$

The cross sections for neutrons, σ_{Kn}, must be deduced from the measured deuterium cross sections:

$$\sigma_{Kd}=\text{“}\sigma_{Kp}\text{”}+\text{“}\sigma_{Kn}\text{”}-\delta\sigma, \tag{11}$$

where $\delta\sigma$ is the screening correction for the deuteron. We have used the notation “σ_{Kp}” and “σ_{Kn}” to indicate that the cross sections σ_{Kp} and σ_{Kn} are smeared by the Fermi motion in the deuteron. The expressions for the pure isotopic-spin cross sections for antiprotons are identical to those for K^- mesons.

A more detailed discussion of the deuteron problem, the effect of Fermi motion, and the screening correction has been given in I. The cross sections smeared out by the Fermi motion were computed from

$$\text{“}\sigma(p)\text{”}=\int|\varphi(q)|^2\sigma(p')d^3q, \tag{12}$$

where p' is the laboratory momentum associated with physical scattering from a free proton, and $\varphi(q)$ is the normalized deuteron wave function in momentum space. The S-wave part of the Moravcsik deuteron wave function was used.[13] The screening correction was obtained from the Glauber-Wilkin expression[14]

$$\delta\sigma=(\langle r^{-2}\rangle/4\pi)\{2\text{“}\sigma_{Kp}\text{”}\,\text{“}\sigma_{Kn}\text{”}(1-\rho_n\rho_p) -\tfrac{1}{2}[\text{“}\sigma_{Kp}\text{”}^2(1-\rho_p{}^2)+\text{“}\sigma_{Kn}\text{”}^2(1-\rho_n{}^2)]\}, \tag{13}$$

where $\langle r^{-2}\rangle$ represents the average inverse square separation of the nucleons in the deuteron, and ρ_p and ρ_n are the ratios of the real to imaginary part of the forward amplitude for scattering from protons and neutrons, respectively. For kaons, the value $\langle r^{-2}\rangle=0.0327$ mb^{-1} was taken from the measurements of

[13] M. Moravcsik, Nucl. Phys. **7**, 113 (1958).
[14] C. Wilkin, Phys. Rev. Letters **17**, 561 (1966).

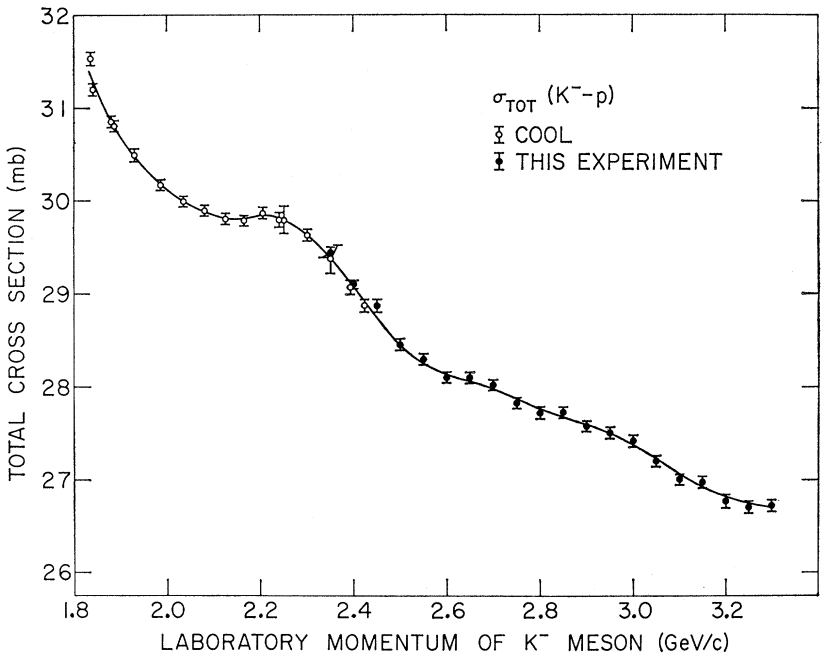

FIG. 5. K^--p total cross sections in the region of the present experiment: 2.35–3.30 GeV/c.

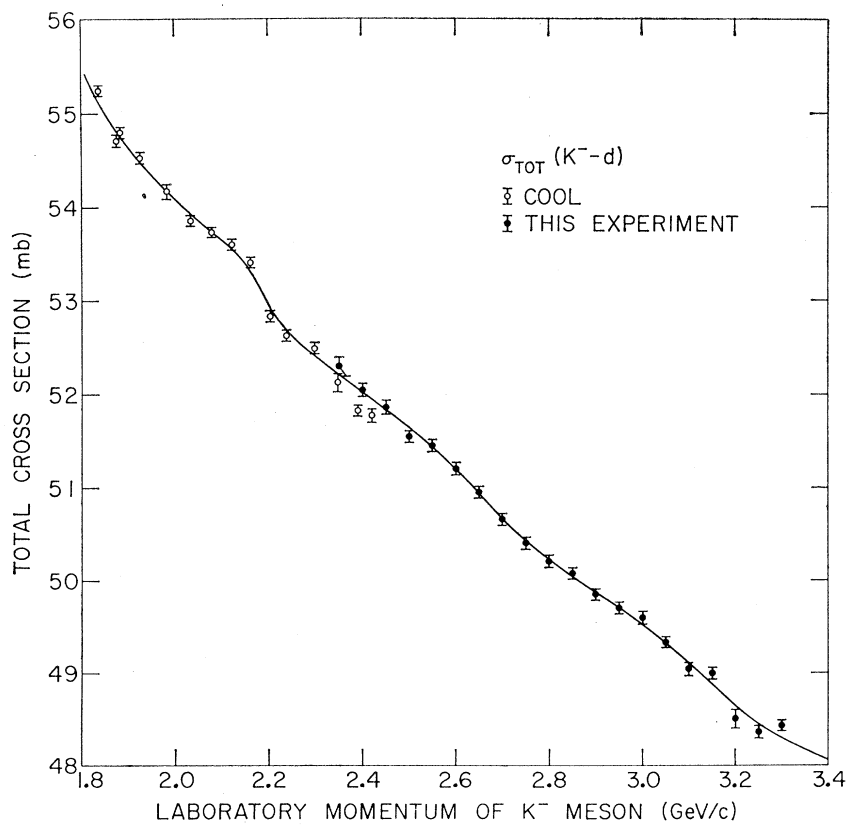

FIG. 6. K^--d total cross sections in the region of the present experiment: 2.35–3.30 GeV/c.

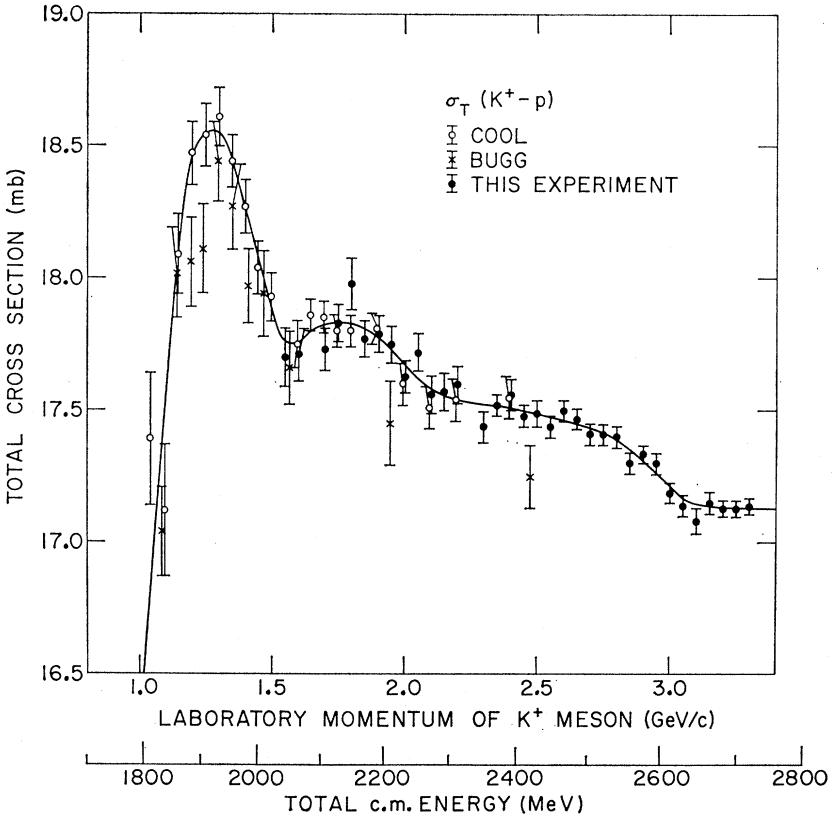

FIG. 7. K^+-p total cross sections, 1.0–3.3 GeV/c.

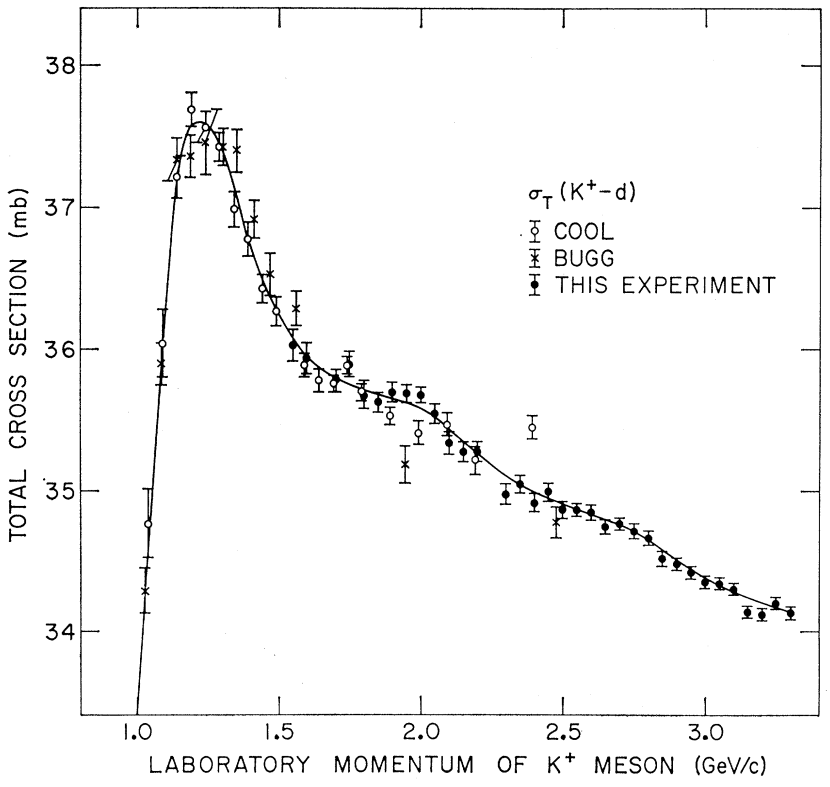

FIG. 8. K^+-d total cross sections, 1.0–3.3 GeV/c.

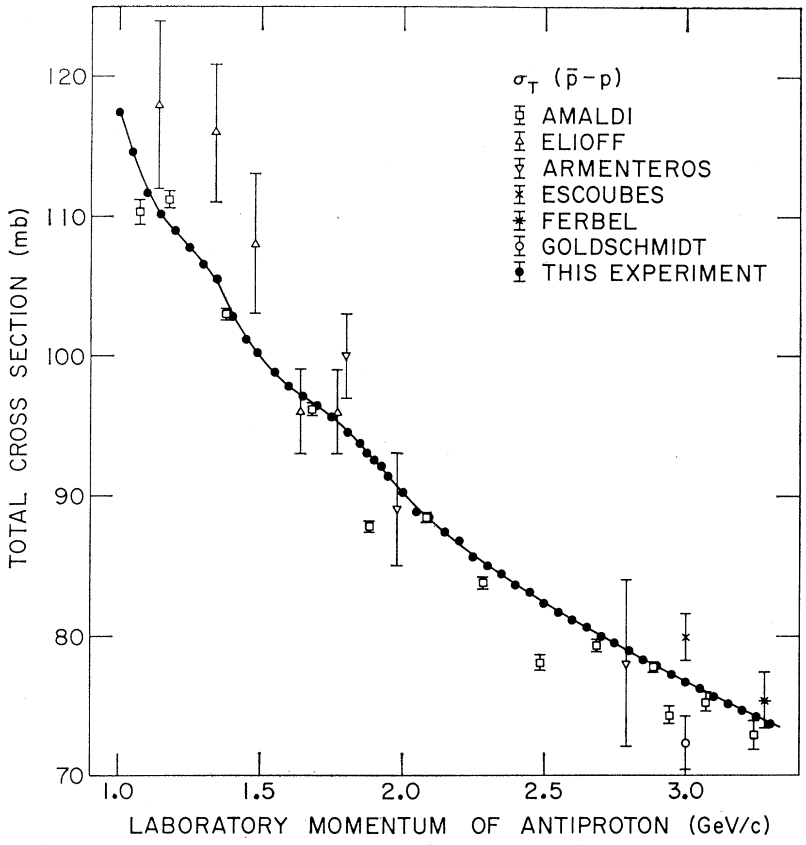

FIG. 9. $\bar{p}$-p total cross sections, 1.0–3.3 GeV/c. For each point, the statistical error is less than the size of the dot.

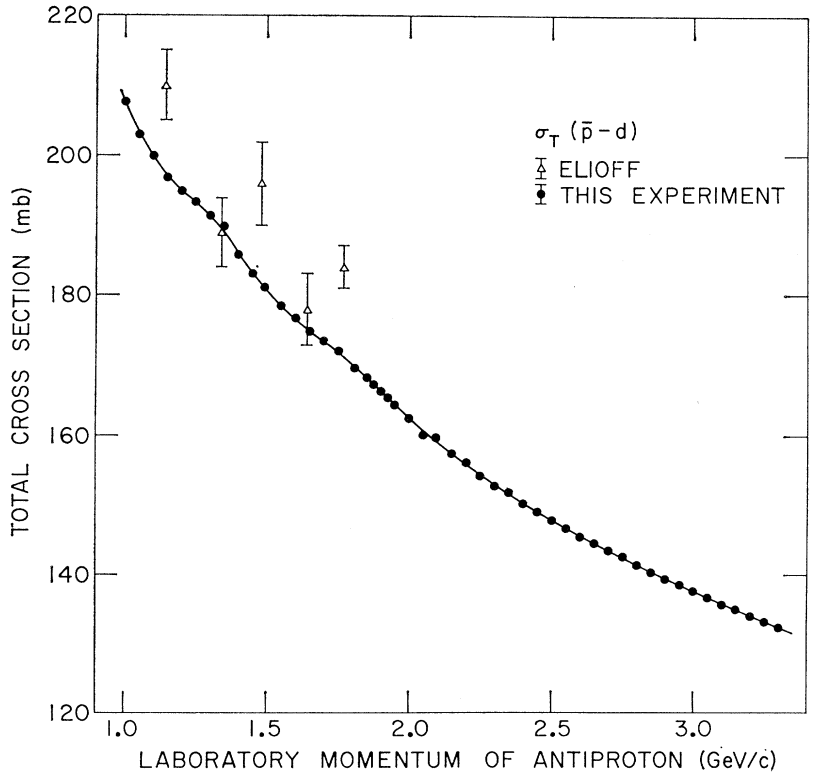

FIG. 10. $\bar{p}$-d total cross sections, 1.0–3.3 GeV/c. For each point, the statistical error is less than the size of the dot.

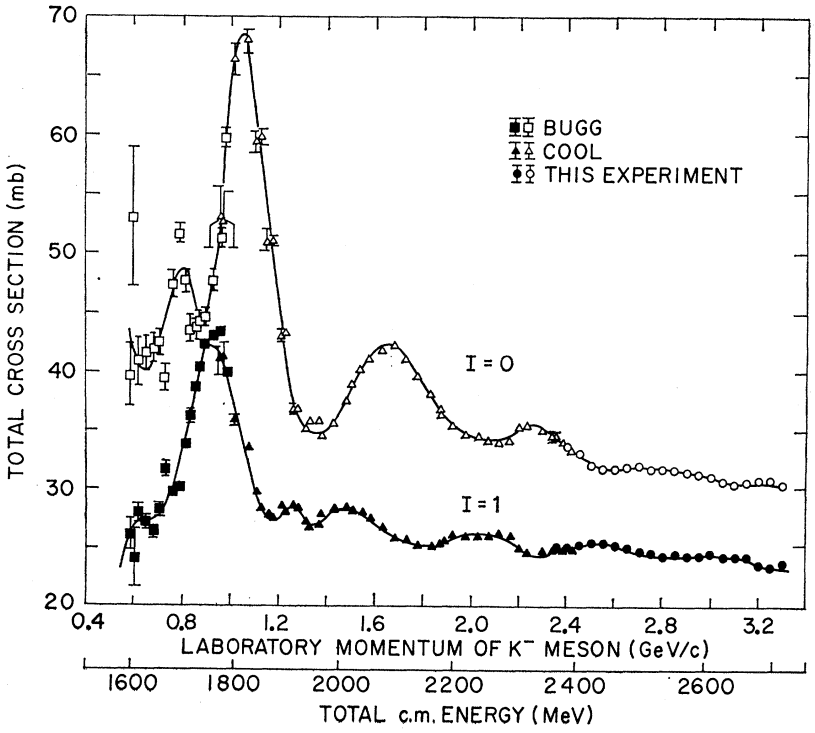

FIG. 11. K^--N total cross sections in the pure $I=1$ and $I=0$ states, 0.6–3.3 GeV/c.

pion total cross sections described in I. For antiprotons, this value was reduced to 0.027 mb^{-1} to account for the sharper t dependence of forward antiproton-nucleon scattering.[15] The values for ρ_p and ρ_n were taken from the literature.[8,16] It was pointed out in the previous section that we were forced to assume $\rho_n=\rho_p$ for antiprotons because of lack of data on this quantity. Typical values of the screening correction are listed in Table I.

The following procedure was used to obtain the pure isotopic-spin cross sections. First, smooth curves were drawn through the proton and deuteron cross-section data. Then the proton curve was smeared out according to (12), and Eqs. (7), (8), (11), and (13) were used to obtain the smeared cross sections "σ_0" and "σ_1" from the deuteron and smeared proton curves. A method of unfolding the Fermi momentum by successive approximations, described in I, was used to obtain smooth curves for the cross sections σ_0 and σ_1. The "data points" for $I=0$ and $I=1$ were obtained by first computing the amount each K^--p and K^--d data point deviated from its smooth curve. These small deviations could then be used to compute a corresponding deviation for pure $I=0$ and $I=1$, neglecting the effects of Fermi motion and screening. The "data point" for $I=0$ or $I=1$ was then computed by adding this small deviation to the value given by the smooth $I=0$ or $I=1$ curve. The "data points" obtained by this method were found to be independent of any reasonable set of smooth curves which were used to compute them. For K^+ mesons, σ_0 was obtained by the same procedure, using Eqs. (9) and (10) instead of (7) and (8). The greatest uncertainty from this procedure was introduced by the method of unfolding. The method has been checked with the pion total cross-section measurements described in I and has proven adequate even for unfolding large structure. Because of the isotopic-spin composition of the deuteron, the statistical uncertainty in the $I=0$ cross sections is always larger than the uncertainty in the $I=1$ cross sections: by a factor of about $\sqrt{5}$ for K^- mesons and antiprotons, and by a factor of about $\sqrt{13}$ for K^+ mesons.

Although the interpretation of a new structure may not be clear, it was assumed to be the effect of a single resonance in order to obtain its resonance parameters. Each new structure, therefore, was fitted with a nonrelativistic Breit-Wigner function superimposed on a smooth background. The Breit-Wigner function was written as

$$\sigma_T(E)=\frac{4\pi\lambda^2}{(2S_a+1)(2S_b+1)}\frac{(2J+1)x}{[(E_R-E)2/\Gamma]^2+1}, \quad (14)$$

where E is the total center-of-mass energy, $\lambda=1/k$, k is

[15] O. Czyzewski, B. Escoubes, Y. Goldschmidt-Clermont, M. Guinea-Moorhead, D. R. O. Morrison, and S. De Unamuno-Escoubes, Phys. Letters 15, 188 (1965).

[16] M. Lusignoli, M. Restignoli, G. Violini, and G. A. Snow, CERN Report No. Th 699, 1966 (unpublished); University of Rome, Nota Interna, No. 109, 1966 (unpublished); and private communication. The real parts of the forward scattering amplitudes given in this report are not in complete agreement with other authors; see, for example, A. A. Carter, University of Cambridge Report No. HEP 68-10 (unpublished); Phys. Rev. Letters 18, 801 (1967).

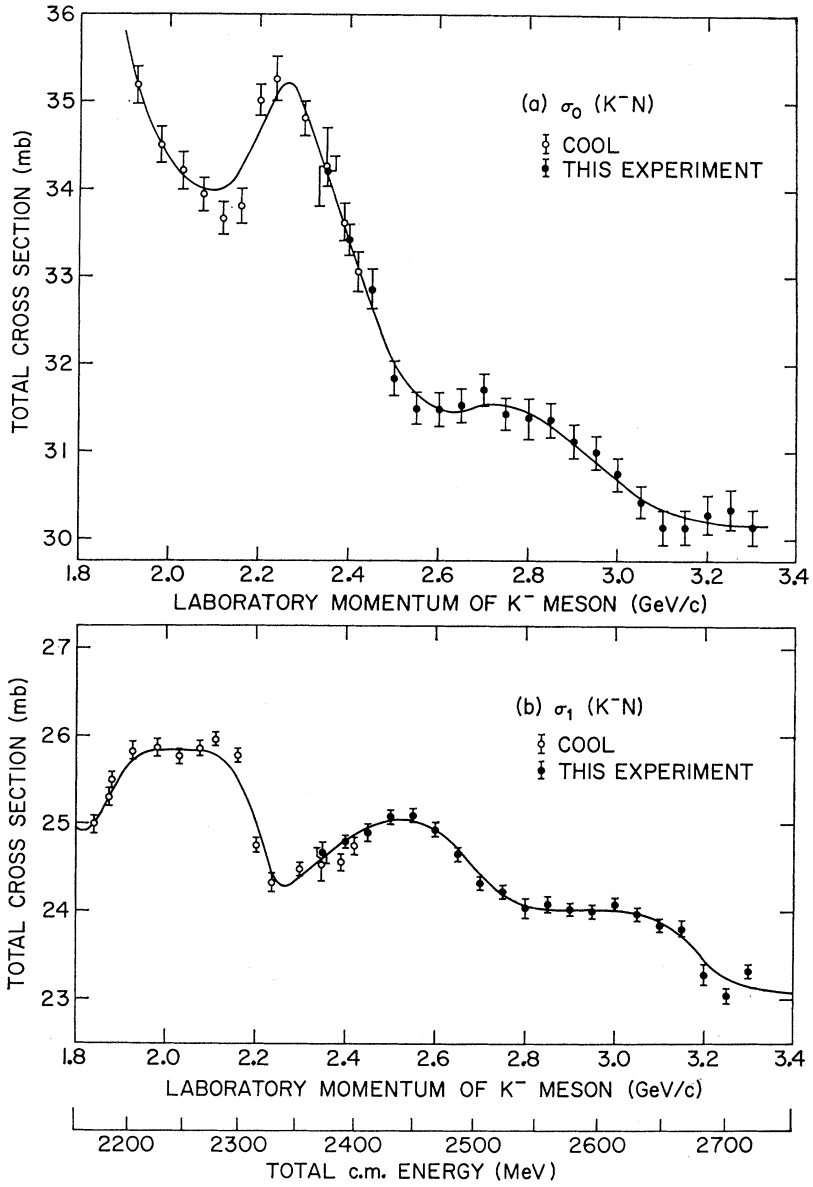

FIG. 12. Detail of the K^--N total cross sections in the region of the present experiment, 2.35–3.30 GeV/c, (a) for $I=0$ and (b) for $I=1$.

the wave number of the incident particle in the center-of-mass system, S_a and S_b are the spins of the incident and target particles, J, E_R, and Γ are the angular momentum, the resonant energy, and the full width at half-height of the resonance, and x is the elasticity of the resonance, defined as its branching ratio for decay into the initial state. An empirical energy dependence for the width Γ was assumed as in I in order to reduce the low-energy tail of the distribution. The smooth background was represented in the fitting as a polynomial in $1/E$. A second approach was also used in the fitting, in which the Breit-Wigner function was subtracted from σ_0 or σ_1, and the resonance parameters varied until a smooth background was obtained.

C. K^--N Total Cross Sections

Figure 11 gives a summary of the K^--N total cross sections of definite isotopic spin in the momentum range 0.6–3.3 GeV/c. The data in the region 0.9–2.4 GeV/c are from I; the data of Bugg *et al.*[17] have been used to show the behavior below 1.0 GeV/c. The data from the present experiment, 2.4–3.3 GeV/c, can be seen more clearly on the expanded scale of Fig. 12 and are listed in Table V.

[17] D. V. Bugg, R. S. Gilmore, K. M. Knight, D. C. Salter G. H. Stafford, E. J. N. Wilson, J. D. Davies, J. D. Dowell, P. M. Hattersley, R. J. Homer, A. W. O'Dell, A. A. Carter, R. J. Tapper, and K. F. Riley, Phys. Rev. **168**, 1466 (1968).

TABLE V. K^-N total cross sections for the $I=0$ and $I=1$ isotopic spin state. Errors represent point-to-point statistical standard deviations. The over-all systematic error, including uncertainties in correcting for screening and Fermi motion in the deuteron, may be as high as ±5%.

Laboratory momentum (GeV/c)	$\sigma_0(K^-N)$ (mb)	$\sigma_1(K^-N)$ (mb)
2.35	34.21±0.18	24.67±0.11
2.40	33.41±0.17	24.79±0.09
2.45	32.84±0.22	24.90±0.10
2.50	31.83±0.19	25.09±0.08
2.55	31.50±0.19	25.10±0.08
2.60	31.48±0.19	24.94±0.08
2.65	31.53±0.19	24.67±0.08
2.70	31.70±0.19	24.34±0.08
2.75	31.43±0.19	24.33±0.08
2.80	31.39±0.22	24.05±0.10
2.85	31.37±0.19	24.09±0.08
2.90	31.12±0.19	24.04±0.08
2.95	31.00±0.19	24.02±0.08
3.00	30.75±0.19	24.09±0.08
3.05	30.42±0.19	23.98±0.08
3.10	30.15±0.19	23.85±0.09
3.15	30.15±0.19	23.81±0.08
3.20	30.29±0.23	23.27±0.12
3.25	30.35±0.22	23.05±0.10
3.30	30.14±0.19	23.32±0.08

TABLE VI. K^+N total cross sections for the $I=0$ isotopic spin state. Also listed are the K^+-neutron total cross sections computed from $\sigma_T(K^+n)=\frac{1}{2}(\sigma_0+\sigma_1)$. Errors represent point-to-point statistical standard deviations. The over-all systematic error, including uncertainties in correcting for screening and Fermi motion in the deutron, may be as high as ±7% for $I=0$ and ±4% for K^+n.

Laboratory momentum (GeV/c)	$\sigma_0(K^+N)$ (mb)	$\sigma_T(K^+n)$ (mb)
1.55	20.11±0.40	18.91±0.16
1.60	20.07±0.37	18.89±0.15
1.70	19.93±0.29	18.83±0.11
1.75	19.89±0.28	18.86±0.11
1.80	19.08±0.36	18.53±0.14
1.85	19.54±0.25	18.66±0.10
1.90	19.59±0.25	18.69±0.10
1.95	19.65±0.24	18.70±0.09
2.00	19.95±0.21	18.79±0.08
2.05	19.37±0.25	18.54±0.10
2.10	19.42±0.26	18.49±0.11
2.15	19.28±0.25	18.43±0.10
2.20	19.21±0.25	18.40±0.10
2.30	19.10±0.23	18.27±0.09
2.35	19.00±0.17	18.26±0.07
2.40	18.62±0.22	18.09±0.08
2.45	19.02±0.16	18.25±0.06
2.50	18.74±0.19	18.11±0.08
2.55	18.90±0.14	18.17±0.06
2.60	18.68±0.16	18.09±0.06
2.65	18.75±0.16	18.02±0.06
2.70	18.80±0.14	18.11±0.06
2.75	18.71±0.16	18.06±0.06
2.80	18.62±0.16	18.01±0.06
2.85	18.60±0.16	17.95±0.06
2.90	18.36±0.12	17.85±0.05
2.95	18.31±0.14	17.81±0.06
3.00	18.42±0.14	17.81±0.06
3.05	18.52±0.14	17.83±0.06
3.10	18.61±0.17	17.85±0.06
3.15	18.07±0.14	17.61±0.06
3.20	18.09±0.12	17.61±0.05
3.25	18.19±0.12	17.66±0.05
3.30	17.95±0.12	17.55±0.05

TABLE VII. $\bar{p}N$ total cross sections for the $I=0$ and $I=1$ isotopic spin states. Errors represent point-to-point statistical standard deviations. The over-all systematic error, including uncertainties in correcting for screening and Fermi motion in the deuteron, may be as high as ±6% for $I=0$ and ±4% for $I=1$.

Laboratory momentum (GeV/c)	$\sigma_0(\bar{p}N)$ (mb)	$\sigma_1(\bar{p}N)$ (mb)
1.00	124.67±0.66	110.17±0.30
1.05	121.40±0.55	107.78±0.26
1.10	115.87±0.52	107.41±0.25
1.15	113.45±0.39	106.66±0.19
1.20	111.19±0.35	106.73±0.17
1.25	108.31±0.33	107.19±0.16
1.30	106.45±0.32	106.49±0.16
1.345	105.56±0.32	105.44±0.16
1.40	102.71±0.30	102.85±0.15
1.45	101.59±0.26	100.65±0.13
1.49	101.60±0.20	98.92±0.11
1.55	100.16±0.20	97.48±0.10
1.60	98.90±0.20	96.72±0.10
1.65	98.26±0.20	95.84±0.10
1.70	97.76±0.20	95.16±0.10
1.75	96.69±0.20	94.53±0.10
1.806	96.15±0.19	92.81±0.09
1.85	95.76±0.20	91.66±0.11
1.875	95.07±0.19	91.03±0.09
1.90	94.76±0.19	90.28±0.09
1.925	94.68±0.19	89.46±0.09
1.95	94.02±0.19	88.74±0.09
2.00	93.00±0.13	87.46±0.07
2.05	91.40±0.17	86.28±0.09
2.095	91.00±0.19	85.92±0.09
2.15	90.32±0.19	84.46±0.09
2.20	90.16±0.19	83.46±0.09
2.25	88.75±0.19	82.49±0.09
2.30	88.49±0.17	81.51±0.09
2.35	87.94±0.17	80.96±0.09
2.40	87.49±0.19	79.83±0.09
2.45	87.31±0.19	79.01±0.09
2.50	86.20±0.13	78.44±0.06
2.55	85.43±0.17	77.85±0.09
2.60	85.17±0.17	77.07±0.09
2.65	84.75±0.16	76.47±0.08
2.70	83.78±0.16	76.02±0.08
2.75	83.46±0.17	75.48±0.09
2.80	83.16±0.16	74.66±0.08
2.85	82.33±0.16	74.09±0.08
2.90	82.10±0.16	73.48±0.08
2.95	81.42±0.16	73.04±0.08
3.00	80.89±0.16	72.47±0.08
3.05	80.88±0.16	71.70±0.08
3.10	80.11±0.16	71.21±0.08
3.15	79.42±0.16	70.90±0.08
3.20	78.96±0.16	70.36±0.08
3.25	78.52±0.16	69.88±0.08
3.30	77.70±0.16	69.64±0.08

For σ_0, in addition to the structure near 2.3 GeV/c [$Y_0^*(2344)$] reported in I, there is a small structure near 2.8 GeV/c. For σ_1, there are two statistically significant structures: one near 2.5 GeV/c and a second near 3.0 GeV/c. The results of fitting Breit-Wigner functions to these three new structures are given in Table VIII (below). We shall refer to them as $Y_0^*(2855)$, $Y_1^*(2455)$, and $Y_1^*(2620)$.

Additional indications for possible high-mass Y^* states of unknown isospin have been found in a K^+

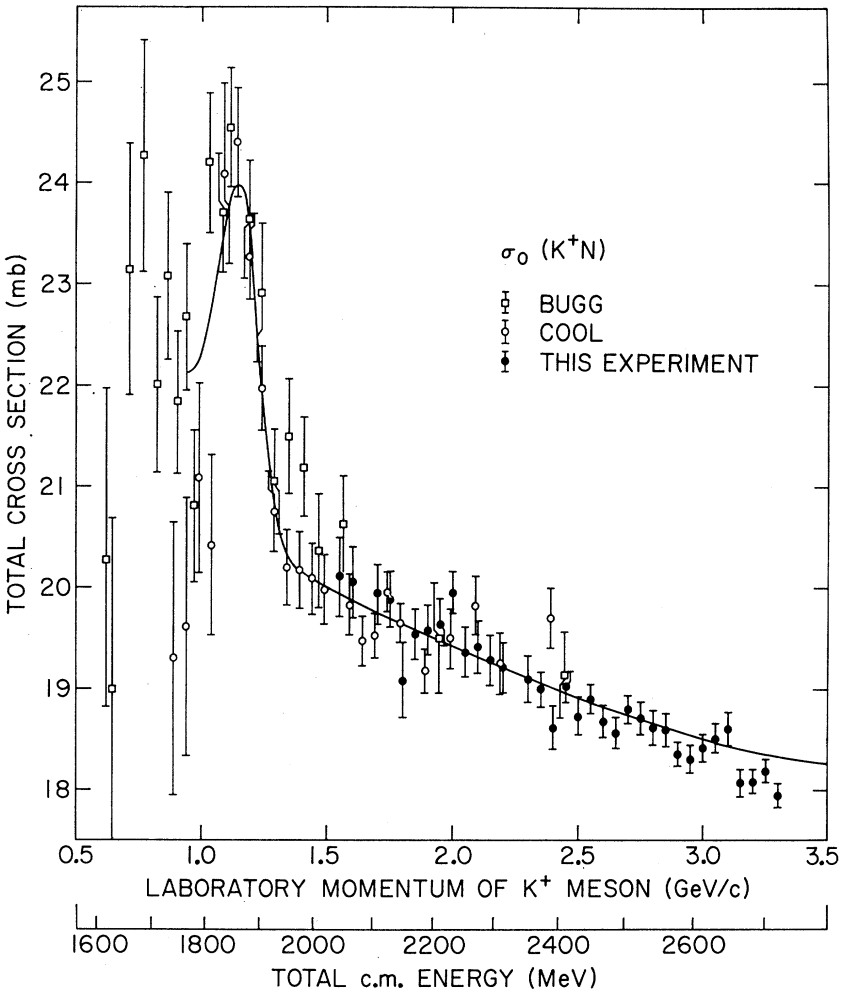

FIG. 13. K^+-N total cross section in the $I=0$ state.

photoproduction experiment.[18] Recent total cross-section measurements at the Rutherford Laboratory[17] confirm the evidence for the $Y_1^*(2455)$.

An attempt was made to locate these new structures on a Regge-trajectory plot. The $Y_0^*(2585)$ could be a recurrence of the $Y_0^*(1520)$ and $Y_0^*(2107)$ and have a

TABLE VIII. Parameters of the observed structures as determined from fitting Breit-Wigner resonance functions. Although the total c.m. energy of each resonance is well determined by the fitting method, the results on the width and height depend sensitively on the type of background used. For the K^-N system a constant background was used: 26.0 mb for $I=0$ and 22.4 mb for $I=1$. For the K^+N system a smooth background which increased with energy but approached a constant asymptotically was assumed: a fourth-degree polynomial in $1/E$,where E is the total c.m. energy. For the $\bar{p}N$ system a smooth background which decreased with energy but approached a constant asymptotically was assumed: a fourth-degree polynomial in $1/E$. *For these particular choices of background,* the statistical uncertainty was typically better than $\pm 30\%$ for the widths and $\pm 15\%$ for the heights.

Notation	S	I	Laboratory momentum (GeV/c)	Total c.m. energy (MeV)	Full c.m. width (MeV)	Height (mb)	$4\pi\lambda^2$ (mb)	$(J+\frac{1}{2})x$
$Y_0^*(2585)$	−1	0	2.92	2585±45	300	4.4	4.4	1.0
$Y_1^*(2455)$	−1	1	2.57	2455±10	140	2.0	5.1	0.39
$Y_1^*(2620)$	−1	1	3.02	2620±15	175	1.3	4.2	0.32
$Z_1^*(2150)$	+1	1	1.80	2150±20	175	0.3	7.9	0.04
$Z_1^*(2500)$	+1	1	2.69	2500±25	160	0.15	4.8	0.03
$\pi_1^*(2190)$	0	1	1.32	2190±10	85	5.5	15.4	0.36
$\pi_1^*(2350)$	0	1	1.77	2350±10	140	3.2	9.8	0.32
$\pi_0^*(2375)$	0	0	1.84	2375±10	190	2.5	9.2	0.27

[18] J. S. Greenberg, V. W. Hughes, D. C. Lu, R. C. Minehart, S. Mori, J. E. Rothberg, and J. Tyson, Phys. Rev. Letters 20, 221 (1968).

spin-parity assignment of $\frac{11}{2}^-$. The $Y_1^*(2455)$ could be a recurrence of the $Y_1^*(1385)$ and have a spin-parity assignment of $\frac{11}{2}^+$. The $Y_1^*(2620)$ could be a recurrence of the $Y_1^*(1770)$ and have a spin-parity assignment of $\frac{13}{2}^-$. The elasticities, in this case, would be of the order of 0.06–0.05. Alternatively, the two new Y_1^*'s could lie on the trajectory starting from the Σ hyperon and have spin-parity assignments of $\frac{9}{2}^+$ and $\frac{11}{2}^-$, respectively.

D. K^+-N Total Cross Sections

The K^+-N cross sections of definite isotopic spin are shown in Figs. 7 and 13 and are listed in Tables III and VI. Table VI also gives a list of K^+-neutron cross sections deduced from σ_0 and σ_1. The $I=0$ total cross section (Fig. 13) is consistent with not having any structure in the momentum range of the present experiment. Two new small structures are present in the $I=1$ cross section (Fig. 7) at about 1.8 and 2.7 GeV/c.

The simplest and most conservative interpretation of these new $I=1$ structures is that they arise from threshold effects of one or several nucleon isobars and/or of K^*'s. If, instead, the two structures were resonances, they have the Breit-Wigner parameters given in Table VIII (below). They would be rather inelastic resonances. They would have the quantum numbers $Y=2$, $S=+1$, and $I=1$; hence, they would be members of the 27 representation of $SU(3)$. The nonrelativistic quark model of elementary particles would require five quarks to form these states.[19]

Additional indications for possible $Y=2$, $S=+1$, $I=1$ states with large masses come from a K^- photoproduction experiment[20] and phase-shift analysis.[21,22]

E. $\bar{p}$-N Total Cross Sections

The $\bar{p}$-N cross sections of definite isotopic spin are shown in Fig. 14 and are listed in Table VII. The $I=0$ data show one structure at a total center-of-mass energy of 2375±10 MeV. The $I=1$ data show two structures at center-of-mass energies of 2190±10 and 2350±10 MeV. The statistical significance of each of these peaks is quite adequate.

The interpretation of these structures is, again, ambiguous between threshold effects and resonances. For instance, the structure at 2190 MeV in $I=1$ could arise from $N_{3/2}^*(1236)$ or $\bar{N}_{3/2}^*(1236)$ production, but its position does not agree with the $N_{3/2}^*(1236)$ threshold effect observed in pp total cross sections.[23] On the other hand, the $\bar{p}p$ single-pion production cross section has been found to rise in this region by an amount

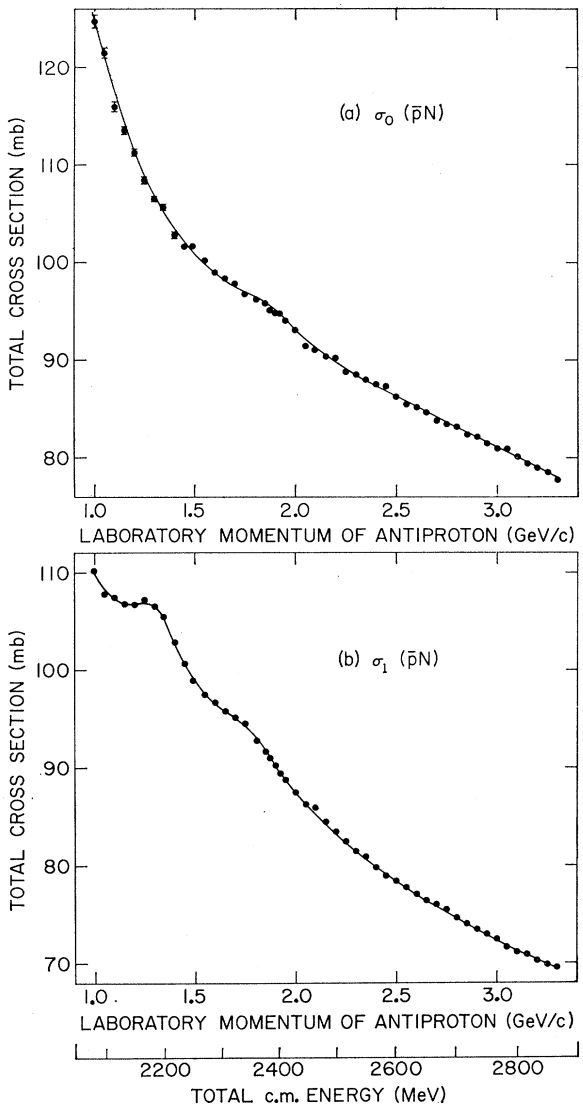

FIG. 14. Antinucleon-nucleon total cross sections, (a) for $I=0$ and (b) for $I=1$.

which could be comparable to the size of this structure.[24] The structures at 2350 MeV in $I=1$ and at 2375 MeV in $I=0$ may arise from the $N_{1/2}^*(1400)$ or $\bar{N}_{1/2}^*(1400)$ threshold. If, on the other hand, these structures are interpreted as nonstrange boson resonances, they would have the Breit-Wigner parameters listed in Table VIII.

Evidence for narrow boson resonances with masses of 2195 and 2382 MeV with $I=1$ or 2 was reported by Chikovani *et al.*[25] They measured the missing-mass (MM) distribution in the reaction $\pi^- + p \rightarrow p + (\mathrm{MM})^-$, where, in the final state, only the recoil proton is ob-

[19] G. Morpurgo, in *Proceedings of the Fourteenth International Conference on High-Energy Physics, Vienna, 1968*, edited by J. Prentki and J. Steinberger (CERN, Geneva, 1968).
[20] J. Tyson, J. S. Greenberg, V. W. Hughes, D. C. Lu, R. C. Minehart, S. Mori, and J. E. Rothberg, Phys. Rev. Letters **19**, 255 (1967).
[21] B. R. Martin, Phys. Rev. Letters **21**, 1286 (1968).
[22] S. Anderson, C. Daum, F. C. Erne, J. P. Lagnaux, J. C. Sens, and F. Udo, Phys. Letters **28B**, 611 (1969).
[23] D. V. Bugg, D. C. Salter, G. H. Stafford, R. F. George, K. F. Riley, and R. J. Tapper, Phys. Rev. **146**, 980 (1966).
[24] W. A. Cooper, L. G. Hyman, W. Manner, B. Musgrave, and L. Voyvodic, Phys. Rev. Letters **20**, 1059 (1968).
[25] G. Chikovani, L. Dubal, M. N. Focacci, W. Kienzle, B. Levrat, B. C. Maglic, M. Martin, C. Nef, P. Schubelin, and J. Seguinot, Phys. Letters **22**, 233 (1966).

TABLE IX. Imaginary part squared of the forward elastic scattering amplitudes for the K^-N system. Results were computed in the center-of-mass frame from the measured total cross sections using the optical theorem. Point-to-point statistical errors are listed; over-all systematic error is ±2% for K^-p and ±5% for K^-n.

Laboratory momentum (GeV/c)	K^-p (mb/sr)	K^-n (mb/sr)
2.35	12.17±0.04	8.54±0.08
2.40	12.20±0.04	8.85±0.06
2.45	12.32±0.06	9.16±0.07
2.50	12.27±0.05	9.54±0.06
2.55	12.43±0.05	9.78±0.06
2.60	12.64±0.05	9.88±0.06
2.65	12.84±0.05	9.90±0.06
2.70	13.06±0.06	9.85±0.06
2.75	13.17±0.06	9.98±0.07
2.80	13.35±0.07	10.05±0.08
2.85	13.65±0.06	10.30±0.07
2.90	13.78±0.06	10.47±0.07
2.95	13.99±0.06	10.67±0.07
3.00	14.18±0.06	10.95±0.07
3.05	14.23±0.06	11.06±0.07
3.10	14.30±0.06	11.15±0.08
3.15	14.55±0.06	11.33±0.08
3.20	14.60±0.08	11.02±0.11
3.25	14.78±0.08	11.01±0.10
3.30	15.08±0.07	11.48±0.08

TABLE X. Imaginary part squared of the forward elastic scattering amplitudes for the K^+N system. Results were computed in the center-of-mass frame from the measured total cross sections using the optical theorem. Point-to-point statistical errors are listed; over-all systematic error is ±2% for K^+p and ±7% for K^+n.

Laboratory momentum (GeV/c)	K^+p (mb/sr)	K^+n (mb/sr)
1.55	2.58±0.03	2.94±0.05
1.60	2.69±0.03	3.06±0.05
1.70	2.92±0.03	3.30±0.04
1.75	3.07±0.02	3.44±0.04
1.80	3.24±0.04	3.44±0.05
1.85	3.28±0.03	3.62±0.04
1.90	3.40±0.03	3.75±0.04
1.95	3.50±0.03	3.89±0.04
2.00	3.57±0.02	4.05±0.03
2.05	3.72±0.03	4.07±0.04
2.10	3.76±0.03	4.17±0.05
2.15	3.88±0.03	4.27±0.05
2.20	4.01±0.03	4.38±0.05
2.30	4.16±0.03	4.56±0.04
2.35	4.31±0.02	4.68±0.04
2.40	4.44±0.03	4.72±0.04
2.45	4.52±0.02	4.92±0.03
2.50	4.63±0.03	4.97±0.04
2.55	4.72±0.02	5.12±0.03
2.60	4.87±0.02	5.20±0.03
2.65	4.96±0.02	5.28±0.04
2.70	5.04±0.02	5.45±0.04
2.75	5.15±0.02	5.55±0.04
2.80	5.26±0.02	5.64±0.04
2.85	5.31±0.02	5.72±0.04
2.90	5.45±0.02	5.77±0.03
2.95	5.53±0.03	5.87±0.04
3.00	5.57±0.03	5.98±0.04
3.05	5.65±0.03	6.12±0.04
3.10	5.72±0.03	6.25±0.04
3.15	5.88±0.03	6.20±0.04
3.20	5.97±0.02	6.31±0.04
3.25	6.08±0.02	6.47±0.04
3.30	6.20±0.02	6.50±0.04

served. While these masses correspond approximately to two of the structures we observed, the reported widths are much smaller. In this energy region, the mass resolution of our apparatus, due to uncertainties in beam momentum and energy loss in the target, was 15 MeV full width at half-height; the 50-MeV/c intervals in momentum between our points correspond to $\Delta M = 18$ MeV. In the region of the 2382-MeV peak, we measured data at 25-MeV/c (9 MeV in the c.m. system) intervals. Further measurements will be necessary to clarify whether the phenomena being observed are the same in these two experiments.

TABLE XI. Imaginary part squared of the forward elastic scattering amplitudes for the $\bar{p}N$ system. Results were computed in the center-of-mass frame from the measured total cross sections using the optical theorem. Point-to-point statistical errors are listed; over-all systematic error is ±2% for $\bar{p}p$ and ±4% for $\bar{p}n$.

Laboratory momentum (GeV/c)	$\bar{p}p$ (mb/sr)	$\bar{p}n$ (mb/sr)
1.00	45.55±0.16	40.10±0.22
1.05	47.07±0.14	41.64±0.20
1.10	48.26±0.14	44.67±0.21
1.15	50.50±0.11	47.48±0.17
1.20	52.99±0.11	50.84±0.16
1.25	55.33±0.10	54.76±0.16
1.30	57.51±0.11	57.53±0.17
1.345	59.58±0.11	59.51±0.18
1.40	60.21±0.11	60.29±0.18
1.45	61.54±0.10	60.97±0.16
1.49	63.08±0.08	61.41±0.14
1.55	65.08±0.08	63.33±0.13
1.60	66.90±0.08	65.41±0.14
1.65	68.97±0.09	67.26±0.14
1.70	71.23±0.09	69.32±0.15
1.75	73.04±0.09	71.40±0.15
1.806	74.70±0.09	72.08±0.14
1.85	76.11±0.10	72.82±0.17
1.875	76.52±0.10	73.23±0.14
1.90	77.11±0.10	73.42±0.15
1.925	77.81±0.10	73.46±0.15
1.95	78.08±0.10	73.64±0.15
2.00	78.94±0.07	74.16±0.12
2.05	79.25±0.09	74.75±0.16
2.095	81.02±0.11	76.44±0.16
2.15	82.01±0.11	76.60±0.16
2.20	83.56±0.12	77.24±0.17
2.25	83.86±0.12	77.84±0.17
2.30	85.20±0.10	78.35±0.17
2.35	86.62±0.10	79.61±0.18
2.40	87.49±0.13	79.67±0.18
2.45	88.91±0.13	80.26±0.18
2.50	89.54±0.09	81.30±0.12
2.55	90.45±0.11	82.25±0.19
2.60	91.66±0.11	82.74±0.19
2.65	92.84±0.12	83.55±0.17
2.70	93.51±0.12	84.65±0.18
2.75	94.79±0.12	85.51±0.20
2.80	95.71±0.12	85.67±0.18
2.85	96.23±0.12	86.36±0.19
2.90	97.39±0.13	86.90±0.19
2.95	98.16±0.13	87.80±0.19
3.00	98.91±0.13	88.35±0.20
3.05	100.02±0.13	88.35±0.20
3.10	100.47±0.13	89.00±0.20
3.15	101.21±0.13	90.06±0.20
3.20	101.90±0.14	90.50±0.21
3.25	102.67±0.14	91.06±0.21
3.30	103.20±0.14	92.22±0.21

Recently a formation experiment was performed with a hydrogen bubble chamber exposed to antiprotons with momenta between 1.1 and 1.5 GeV/c.[26] The authors of the experiment suggest that the $I=1$ structure at 2190 MeV may be due to a formation of a $\rho\rho\pi$ resonance of width $20<\Gamma<80$ MeV. Fits to the recently measured differential cross sections for $\bar{p}p \to \pi^+\pi^-$ and K^+K^- are consistent with two $I=1$ resonances: one with $J=3$ near 2120 MeV and a second with $J=5$ near 2290 MeV.[27] The authors state that, in view of uncertainties in the mass determination, further analysis is needed to establish whether these may be related to the two structures in the $I=1$ total cross sections.

It might be interesting to conjecture that the structures observed in this total cross-section measurement are indeed pionic resonances and to attempt to locate them on a Regge-trajectory plot. Since the spin-parity assignments for most of the high-mass states are not known, this plot, of course, must be considered highly speculative. It would seem that, on the same trajectory, neighboring resonances are spaced by one unit of spin and that they alternate in parity (exchange degeneracy). The structures reported in the present experiment would have spin 5 and 6; therefore, they would have elasticities of about 4–6%. Elasticity in this context means a branching ratio of $\pi^* \to N\bar{N}$.

[26] G. R. Klabfleisch, R. C. Strand, and V. Vanderburg, Phys. Letters **29B**, 259 (1969).

[27] H. Nicholson, B. C. Barish, J. Pine, A. V. Tollestrup, J. K. Yoh, C. Delorme, F. Lobkowicz, A. C. Melissinos, Y. Nagashima, A. S. Carroll, and R. H. Phillips, Phys. Rev. Letters **23**, 603 (1969).

F. Imaginary Parts of Forward Scattering Amplitudes

For completeness, we have computed as in I the imaginary parts squared for the forward elastic scattering from the cross sections observed in the present experiment, using the optical theorem. These quantities, given in the center-of-mass frame for the $K^{\pm}$-N and $\bar{p}$-N systems, are listed in Tables IX–XI.

ACKNOWLEDGMENTS

We wish to thank Dr. G. K. Green, Dr. J. R. Sanford, T. Blair, and the AGS staff for their support. We thank Dr. C. Wilkin and Dr. R. F. Peierls for useful discussions. The cooperation of A. P. Schlafke and the Cryogenic Group is greatly appreciated. We also wish to acknowledge the technical assistance of P. Anzoli, G. Munoz, H. Sauter, F. Seier, and O. Thomas.